LETTER

doi:10.1038/nature09915

Modelling schizophrenia using human induced pluripotent stem cells

Kristen J. Brennand[1], Anthony Simone[1]*, Jessica Jou[1]*, Chelsea Gelboin-Burkhart[1]*, Ngoc Tran[1]*, Sarah Sangar[1], Yan Li[1], Yangling Mu[1], Gong Chen[2], Diana Yu[1], Shane McCarthy[3], Jonathan Sebat[4] & Fred H. Gage[1]

Schizophrenia (SCZD) is a debilitating neurological disorder with a world-wide prevalence of 1%; there is a strong genetic component, with an estimated heritability of 80–85%[1]. Although post-mortem studies have revealed reduced brain volume, cell size, spine density and abnormal neural distribution in the prefrontal cortex and hippocampus of SCZD brain tissue[2] and neuropharmacological studies have implicated dopaminergic, glutamatergic and GABAergic activity in SCZD[3], the cell types affected in SCZD and the molecular mechanisms underlying the disease state remain unclear. To elucidate the cellular and molecular defects of SCZD, we directly reprogrammed fibroblasts from SCZD patients into human induced pluripotent stem cells (hiPSCs) and subsequently differentiated these disorder-specific hiPSCs into neurons (Supplementary Fig. 1). SCZD hiPSC neurons showed diminished neuronal connectivity in conjunction with decreased neurite number, PSD95-protein levels and glutamate receptor expression. Gene expression profiles of SCZD hiPSC neurons identified altered expression of many components of the cyclic AMP and WNT signalling pathways. Key cellular and molecular elements of the SCZD phenotype were ameliorated following treatment of SCZD hiPSC neurons with the antipsychotic loxapine. To date, hiPSC neuronal pathology has only been demonstrated in diseases characterized by both the loss of function of a single gene product and rapid disease progression in early childhood[4–6]. We now report hiPSC neuronal phenotypes and gene expression changes associated with SCZD, a complex genetic psychiatric disorder.

Four SCZD patients were selected: patient 1, diagnosed at 6 years of age, had childhood-onset SCZD; patients 2, 3 and 4 were from families in which all offspring and one parent were affected with psychiatric disease (Supplementary Fig. 3a). Primary human fibroblasts were reprogrammed using inducible lentiviruses[7]. Control and SCZD hiPSCs expressed endogenous pluripotency genes, repressed viral genes and were indistinguishable in assays for self-renewal and pluripotency (Fig. 1 and Supplementary Fig. 2). SCZD hiPSCs had no apparent defects in generating neural progenitor cells (NPCs) or neurons (Fig. 1 and Supplementary Fig. 3). Most hiPSC neurons were presumably glutamatergic and expressed VGLUT1 (also known as SLC17A7; Supplementary Fig. 8a). Approximately 30% of neurons were GAD65/67-positive (also known as GAD1/2; GABAergic) (Supplementary Fig. 8c, d) whereas less than 10% of neurons were tyrosine hydroxylase-positive (dopaminergic) (Supplementary Fig. 7).

Neuronal connectivity was assayed using trans-neuronal spread of rabies; *in vivo*, rabies transmission occurs via synaptic contacts and is strongly correlated with synaptic input strength[8]. Primary infection was restricted by replacing the rabies coat protein with envelope A (ENVA), which infects only via the avian tumour virus A (TVA) receptor; viral spread was limited to monosynaptically connected neurons by deleting the rabies glycoprotein gene (ΔG)[9]. Neurons were first transduced with a lentivirus expressing histone 2B (H2B)–green fluorescent protein (GFP) fusion protein, TVA and G from the synapsin (SYN) promoter (LV-SYNP-HTG). One week later, neurons were transduced with modified rabies virus (Rabies-ENVAΔG-RFP). Primary infected cells were positive for both H2B–GFP and RFP (red fluorescent protein); neurons monosynaptically connected to primary cells were GFP-negative but RFP-positive (Supplementary Fig. 4a). Transduction with Rabies-ENVAΔG-RFP alone resulted in no RFP-positive cells, whereas transduction with Rabies-ENVAΔG-RFP following lentiviral transduction without rabies glycoprotein (SYNP-HT) led to only single GFP^+RFP^+ cells, indicating that *in vitro* rabies infection and spread are dependent on TVA expression and G trans-complementation, respectively (Supplementary Fig. 4c, d).

There was decreased neuronal connectivity in SCZD hiPSC neurons (Fig. 2; Supplementary Figs 4b, c, 5 and 6). Fluorescence-activated cell sorting (FACS) analysis confirmed differences in neuronal connectivity and demonstrated that comparable numbers of βIII-tubulin-positive neurons were labelled with LV-SYNP-HTG. Though the mechanism of rabies trans-neuronal tracing is not fully understood, the presynaptic protein NCAM has been implicated[10]; *NCAM* expression is decreased in SCZD hiPSC neurons (Supplementary Table 3). Rabies trans-neuronal tracing occurs in functionally immature hiPSC neurons (Supplementary Fig. 4e) and in the presence of the voltage-gated sodium channel blocker tetrodotoxin (TTX) (1 μM), depolarizing KCl (50 mM) or the calcium channel blocker ryanodine (10 μM) (Supplementary Fig. 4f). Decreased

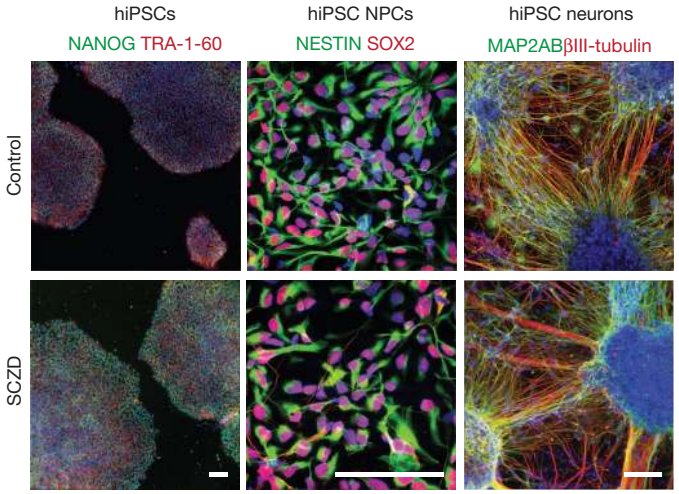

Figure 1 | Patient-specific hiPSCs, NPCs and neurons. Left, hiPSCs express NANOG (green) and TRA-1-60 (red). DAPI (blue). ×100, scale bar 100 μm. Centre, hiPSC neural progenitor cells (NPCs) express NESTIN (green) and SOX2 (red). DAPI (blue). ×600, scale bar 100 μm. Right, hiPSC neurons express βIII-tubulin (red) and the dendritic marker MAP2AB (green). DAPI (blue). ×200, scale bar 100 μm.

[1]Salk Institute for Biological Studies, Laboratory of Genetics, 10010 North Torrey Pines Road, La Jolla California 92037, USA. [2]Department of Biology, Pennsylvania State University, 201 Life Science Building, University Park, Pennsylvania 16802, USA. [3]Cold Spring Harbor Laboratory, 1 Bungtown Road, Cold Spring Harbor, New York 11724, USA. [4]University of California San Diego, Department of Psychiatry and Department of Cellular and Molecular Medicine, University Of California, San Diego, La Jolla, California 92093, USA.
*These authors contributed equally to this work.

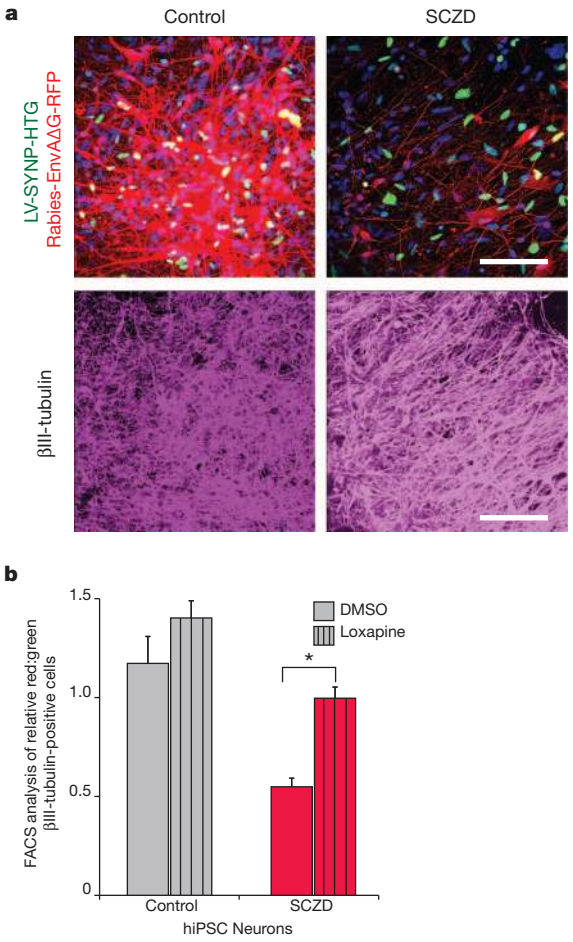

Figure 2 | Decreased neuronal connectivity in SCZD hiPSC neurons. **a**, Representative images of control and SCZD hiPSC neurons cotransduced with LV-SYNP-HTG and Rabies-ENVAΔG-RFP, 10 days post rabies transduction. All images were captured using identical laser power and gain settings. βIII-tubulin staining (purple) of the field is shown below each panel. ×400, scale bar 80 μm. **b**, Graph showing treatment of SCZD hiPSC neurons with Loxapine resulted in a statistically significant improvement in neuronal connectivity. Error bars are s.e., $*P < 0.05$.

trans-neuronal tracing is evidence of decreased neuronal connectivity, but not necessarily decreased synaptic function, in SCZD hiPSC neurons.

We tested the ability of five antipsychotic drugs to improve neuronal connectivity *in vitro*. Clozapine, loxapine, olanzapine, risperidone and thioridazine were administered for the final 3 weeks of neuronal differentiation. Only loxapine significantly increased neuronal connectivity in hiPSC neurons from all patients (Fig. 2b and Supplementary Fig. 5). Optimization of the concentration and timing of drug administration may improve the effects of the other antipsychotic medications.

Reduced dendritic arborization has been observed in post-mortem SCZD brains[11] and in animal models[12]. SCZD hiPSC neurons show a decrease in the number of neurites (Fig. 3a and Supplementary Fig. 9a, b). Synaptic genes are associated with SCZD[13] (Supplementary Fig. 9d) and impaired synaptic maturation occurs in a number of mouse models[12]. hiPSC neurons express dense puncta of synaptic markers that co-stain for both pre- and post-synaptic markers (Supplementary Fig. 8a, b). Whereas we observed decreased PSD95 protein (also known as DLG4, levels relative to microtubule associated protein 2ab (MAP2AB) in SCZD hiPSC neuronal dendrites (Fig. 3b; Supplementary Fig. 9h), the levels of SYN, VGLUT1, GLUR1 (also known as GRIA1), VGAT (also known as SLC32A1) and GEPH (also known as GPHN) were unaffected (Supplementary Fig. 9e–j). Decreased PSD95 synaptic density in SCZD hiPSC neurons failed to reach statistical significance (Fig. 3c and Supplementary Fig. 9c).

We used electrophysiology and calcium transient imaging to measure spontaneous neuronal activity (Fig. 3d–k and Supplementary Fig. 10). SCZD hiPSC neurons showed normal transient inward sodium currents and sustained outward potassium currents in response to membrane depolarizations (Fig. 3d), action potentials to somatic current injections (Fig. 3e), spontaneous excitatory postsynaptic currents (EPSCs) (Fig. 3f) and spontaneous inhibitory postsynaptic currents (IPSCs) (Fig. 3g). The amplitude and rate of spontaneous calcium transients were unaffected (Fig. 3h–j and Supplementary Fig. 10a–d) and there was no difference in synchronicity of spontaneous calcium transients (Fig. 3k and Supplementary Fig. 10e–g).

Increased *NRG1* expression has been observed in post-mortem SCZD brain tissue[13]. *NRG1* expression was increased in SCZD hiPSC neurons (Fig. 4d–f) but not SCZD fibroblasts, hiPSCs or NPCs (Fig. 4e), demonstrating the importance of studying gene expression changes in the cell type relevant to disease. In all, 596 unique genes (271 upregulated and 325 downregulated) showed greater than 1.30-fold-expression changes between SCZD and control hiPSC neurons ($P < 0.05$) (Supplementary Fig. 11a, b and Supplementary Table 3). Of these genes, 13% (74) have published associations with SCZD and 16% (96) have been linked to SCZD by post-mortem gene expression profiles available through the Stanley Medical Research Institute[14] (Supplementary Table 3); in total 25% (149) of our differentially expressed genes have been previously implicated in SCZD. Gene ontology (GO) analysis identified significant perturbations of glutamate, cAMP and WNT signalling (Fig. 4a–c, Supplementary Table 4 and Supplementary Fig. 11c), pathways required for activity-dependent refinement of synaptic connections and long-term potentiation[15–17]. Sixteen of 17 candidate genes from these families were validated by quantitative PCR (Supplementary Table 2; Fig. 4f and Supplementary Fig. 11e).

Copy number variants (CNVs) are rare, highly penetrant structural disruptions. SCZD patients have a 1.15-fold increase in CNV burden, but how this translates into illness is unknown. Patient 4 had four CNVs involving genes previously associated with SCZD or bipolar disorder (BD)[13,18,19]; of these, neuronal expression of *NRG3* and *GALNT11*, but not of *CYP2C19* or *GABARB2*/*GABARA6* (also known as *GABRB2* and *GABRA6*, respectively) was affected (Supplementary Fig. 12 and Supplementary Table 5). A second analysis of CNVs unbiased by previous genome wide association studies (GWAS) identified 42 genes affected by CNVs in our four SCZD patients (Supplementary Table 5). Although twelve of these genes showed altered neuronal expression consistent with genotype ($P < 0.05$), most changes were extremely small and only three (*CSMD1*, *MYH1*, *MYH4*) showed >1.3-fold effects (Supplementary Table 5). Well-established SCZD CNVs occur at 1q21.1, 15q11.2, 15q13.3, 16p11.2 and 22q11.2 (refs 13, 18, 19), but the relevant genes remain unidentified. Our patients had no evidence of CNVs at these regions, and gene expression of the best candidate genes in each region, such as *GJA8* (1q21.1), *CYFIP1* (15q11.1), *CHRFAM7A* (15q13.3), *PRODH* (22q11.2), *COMT* (22q11.2) and *ZDHHC8* (22q11.2)[18,20], was not affected in our SCZD hiPSC neurons (Supplementary Table 6).

Consistent with published reports, loxapine increased *NRG1* expression in neurons[21]. Loxapine also increased expression of several glutamate receptors, including *GRIK1*, *GRM7* and *GRIN2A*, and ameliorated expression of *ADCY8*, *PRKCA*, *WNT7A* and *TCF4* (Fig. 4f and Supplementary Fig. 11e).

SCZD hiPSC neurons from heterogeneous patients had similar deficits, replicating some but not all aspects of the cellular and molecular phenotypes observed in post-mortem human studies and animal models (Supplementary Table 1). We observed decreased neuronal connectivity in SCZD hiPSC neurons, but not defects in synaptic function; this may reflect technical limitations of our synaptic activity assays. Due to the heterogeneity of our patient cohort and small sample size, our findings might not generalize to all subtypes of SCZD and our microarray

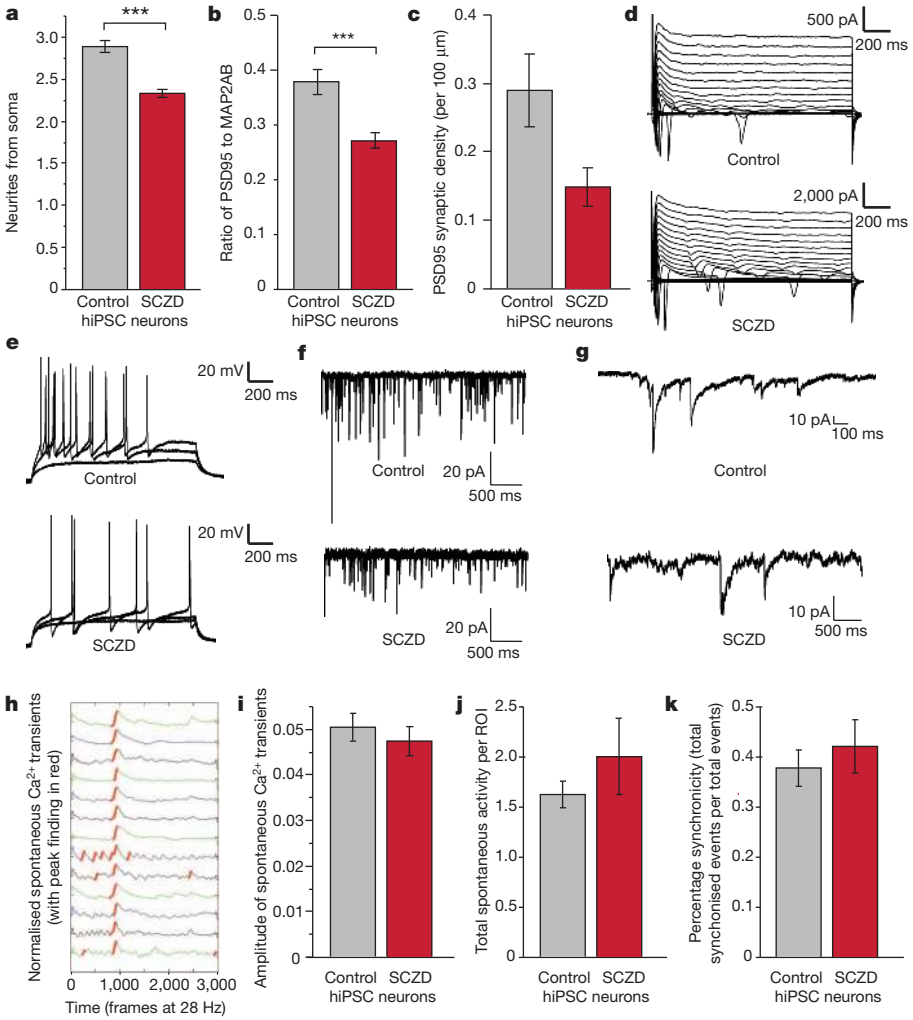

Figure 3 | Decreased neurites and synaptic protein levels but normal electrophysiological and spontaneous calcium transient activity in SCZD hiPSC neurons. **a**, Decreased neurites in SCZD hiPSC neurons. **b**, Decreased PSD95 protein relative to MAP2AB for SCZD hiPSC neurons. **c**, Trend of decreasing PSD95 synaptic density in SCZD hiPSC neurons. **d**–**g**, Electrophysiological characterization. hiPSC neurons grown on astrocytes show normal sodium and potassium currents when voltage-clamped (**d**), normal induced action potentials when current-clamped (**e**), and spontaneous excitatory (**f**) and inhibitory (**g**) synaptic activity. **h**–**k**, Spontaneous calcium transient imaging. Representative spontaneous Fluo-4AM calcium traces of fluorescent intensity versus time generated from 3-month-old hiPSC neurons (**h**). There is no difference between the spike amplitude of spontaneous calcium transients of control and SCZD hiPSC neurons (**i**), no difference between the total numbers of spontaneous calcium transients per total number of regions of interest in cultures of control and SCZD hiPSC neurons (**j**), and no change in percentage synchronicity per calcium transient in control and SCZD hiPSC neurons (**k**). Error bars are s.e., $***P < 0.001$.

comparisons of SCZD and control hiPSC neurons are necessarily preliminary. Gene expression studies of hiPSC neurons permit straightforward comparisons of antipsychotic treatments on live, genetically identical neurons from patients with known clinical treatment outcomes, eliminating many confounding variables of post-mortem analysis such as treatment history, drug or alcohol abuse, and cause of death. For example, although loxapine is characterized as a high affinity antagonist of serotonin 5-HT_2 receptors and dopamine D1, D2 and D4 receptors[22], treatment of SCZD hiPSC neurons resulted in altered gene expression and increased neuronal connectivity.

Of the 596 unique genes differentially expressed in our SCZD hiPSC neurons (>1.30-fold, $P < 0.05$), 25% have been previously implicated in SCZD (Supplementary Table 3). Although our gene expression profiles of SCZD hiPSC neurons confirm and extend the major hypotheses generated by pharmacological and GWAS studies of SCZD, they also identify some pathways not before linked to SCZD, such as NOTCH signalling, SLIT/ROBO axon guidance, EFNA mediated axon growth, cell adhesion and transcriptional silencing (Supplementary Table 4). Many of the genes most affected in SCZD hiPSC neurons belong to pathways previously associated with SCZD, although they have not yet been singled out as SCZD genes. For example, whereas *PDE4B* is a well-characterized SCZD gene, we observed significant misexpression of *PDE1C*, *PDE3A*, *PDE4D*, *PDE4DIP*, *PDE7B*, *ADCY7* and *ADCY8*. Additionally, although some key SCZD/BD genes, including *NRG1* and *ANK3*, were misexpressed in all of our SCZD hiPSC neurons, many others, including *ZNF804A*, *GABRB1*, *ERBB4*, *DISC1* and *PDE4B*, were aberrantly expressed in some but not all patients (Fig. 4d). Our data support the "watershed model"[23] of SCZD whereby many different combinations of gene misfunction may disrupt the key pathways affected in SCZD. We predict that, as the number of SCZD cases studied using hiPSC neurons increases, a diminishing number of genes will be consistently affected across the growing patient cohort; instead, evidence will accumulate that a handful of essential pathways can be disrupted in diverse ways to result in SCZD.

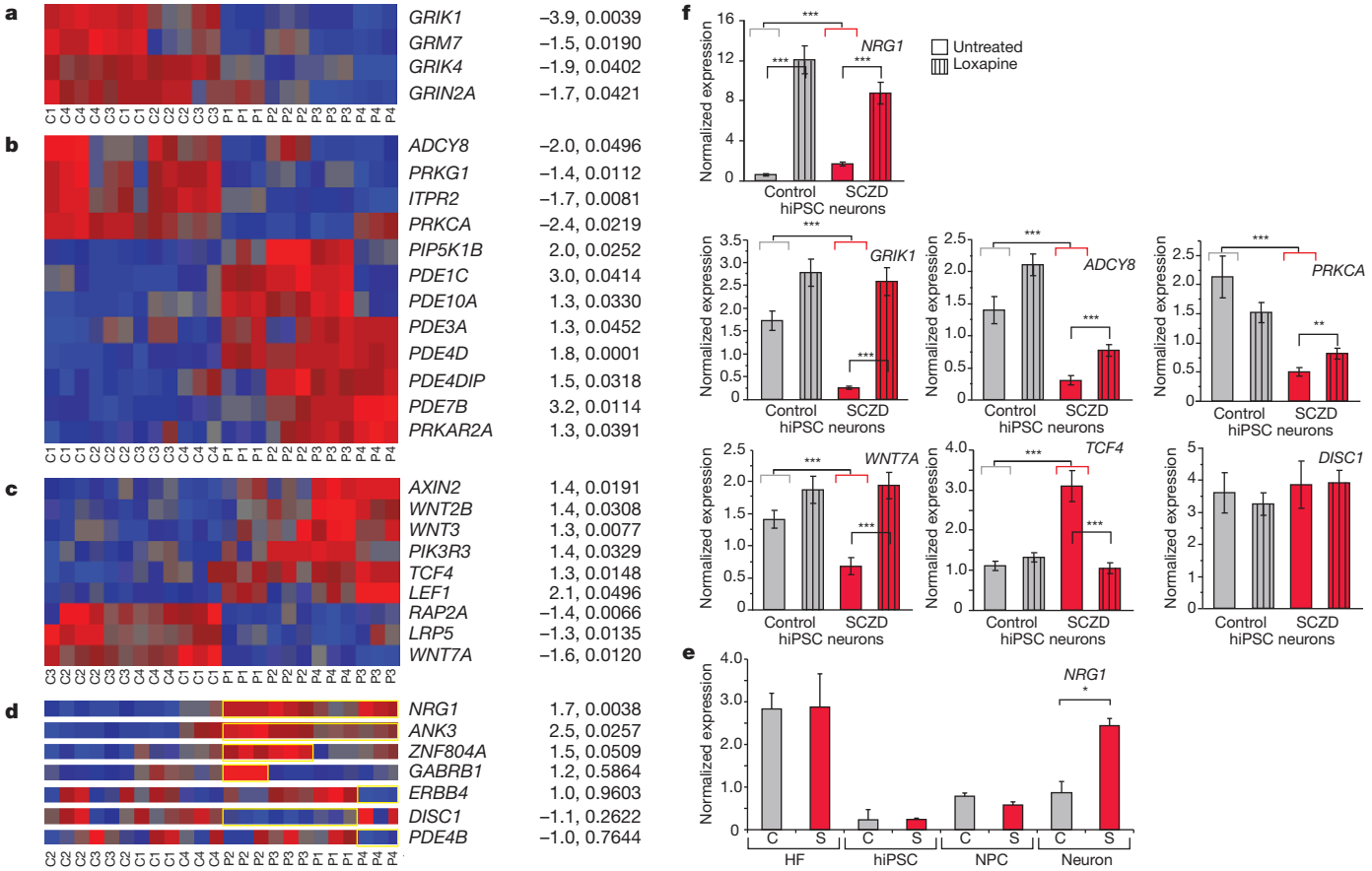

Figure 4 | RNA expression analysis of control and SCZD hiPSC neurons. **a**–**c**, Heat maps showing microarray expression profiles of altered expression of glutamate receptors (**a**), cAMP signalling (**b**) and WNT signalling (**c**) genes in SCZD hiPSC neurons. Fold-change and *P*-values (diagnosis) are shown on the right. **d**, Heat maps showing perturbed expression (highlighted in yellow) of *NRG1* and *ANK3* in all four SCZD patients, as well as altered expression of *ZNF804A*, *GABRB1*, *ERBB4*, *DISC1* and *PDE4B* in some but not all patients. Fold-change and *P*-values (diagnosis) are shown on the right. **e**, Altered expression of *NRG1* is detected in SCZD hiPSC neurons but not in patient fibroblasts, hiPSCs or hiPSC NPCs. C, control; S, SCZD. **f**, qPCR validation of altered expression of *NRG1*, *GRIK1*, *ADCY8*, *PRKCA*, *WNT7A*, *TCF4* and *DISC1*, as well as response to 3 weeks of treatment with loxapine (striped bars) in 6-week-old hiPSC neurons. $*P < 0.05$, $**P < 0.01$, $***P < 0.001$.

METHODS SUMMARY

Reprogramming hiPSCs. Control and SCZD human fibroblasts were obtained from cell repositories and were reprogrammed with tetracycline-inducible lentiviruses expressing the transcription factor genes *OCT4* (also known as *POU5F1*), *SOX2*, *KLF4*, *cMYC* and *LIN28* (ref. 7). Lentiviruses were packaged in 293T HEK cells transfected with polyethylenimine (PEI) (Polysciences). Human fibroblasts were transduced and then split onto mouse embryonic fibroblasts (mEFs). Cells were switched to HUES medium (KO-DMEM (Invitrogen), 10% KO-Serum Replacement (Invitrogen), 10% Plasminate (Talecris), 1× GlutaMAX (Invitrogen), 1× NEAA (Invitrogen), 1× 2-β-mercaptoethanol (Sigma) and 20 ng ml^{-1} FGF2 (Invitrogen)) and 1 μg ml^{-1} doxycycline (Sigma) was added to HUES medium for the first 21–28 days of reprogramming. hiPSCs were generally grown in HUES medium: early passage hiPSCs were split through manual passaging, whereas at higher passages hiPSCs could be enzymatically passaged with 1 mg ml^{-1} collagenase (Sigma).

hiPSC differentiation to NPCs and neurons. Embryoid bodies were generated from hiPSCs and then transferred to non-adherent plates (Corning). Colonies were maintained in suspension in N2 medium (DMEM/F12 (Invitrogen), 1× N2 (Invitrogen)) for 7 days and then plated onto polyornithine (PORN)/laminin-coated plates. Visible rosettes formed within 1 week and were manually dissected and cultured in NPC medium (DMEM/F12, 1× N2, 1× B27-RA (Invitrogen), 1 μg ml^{-1} laminin (Invitrogen) and 20 ng ml^{-1} FGF2 (Invitrogen). NPCs are maintained at high density, grown on PORN/laminin-coated plates in NPC medium and split approximately 1:4 every week with Accutase (Millipore). For neural differentiations, NPCs were dissociated with Accutase and plated at low density in neural differentiation medium (DMEM/F12-Glutamax, 1× N2, 1× B27-RA, 20 ng ml^{-1} BDNF (Peprotech), 20 ng ml^{-1} GDNF (Peprotech), 1 mM dibutyryl-cyclic AMP (Sigma), 200 nM ascorbic acid (Sigma) onto PORN/laminin-coated plates.

Assays for neuronal connectivity, neurite outgrowth, synaptic protein expression, synaptic density, electrophysiology, spontaneous calcium transient imaging and gene expression were used to compare control and SCZD hiPSC neurons.

Full Methods and any associated references are available in the online version of the paper at www.nature.com/nature.

Received 26 July 2010; accepted 10 February 2011.
Published online 13 April 2011.

1. Sullivan, P. F., Kendler, K. S. & Neale, M. C. Schizophrenia as a complex trait: evidence from a meta-analysis of twin studies. *Arch. Gen. Psychiatry* **60,** 1187–1192 (2003).
2. Wong, A. H. & Van Tol, H. H. Schizophrenia: from phenomenology to neurobiology. *Neurosci. Biobehav. Rev.* **27,** 269–306 (2003).
3. Javitt, D. C., Spencer, K. M., Thaker, G. K., Winterer, G. & Hajos, M. Neurophysiological biomarkers for drug development in schizophrenia. *Nature Rev. Drug Discov.* **7,** 68–83 (2008).
4. Ebert, A. D. *et al.* Induced pluripotent stem cells from a spinal muscular atrophy patient. *Nature* **457,** 277–280 (2009).
5. Lee, G. *et al.* Modelling pathogenesis and treatment of familial dysautonomia using patient-specific iPSCs. *Nature* **461,** 402–406 (2009).
6. Marchetto, M. C. *et al.* A model for neural development and treatment of Rett syndrome using human induced pluripotent stem cells. *Cell* **143,** 527–539 (2010).
7. Maherali, N. *et al.* Directly reprogrammed fibroblasts show global epigenetic remodeling and widespread tissue contribution. *Cell Stem Cell* **1,** 55–70 (2007).
8. Ugolini, G. Use of rabies virus as a transneuronal tracer of neuronal connections: implications for the understanding of rabies pathogenesis. *Dev. Biol. (Basel)* **131,** 493–506 (2008).

9. Wickersham, I. R. *et al.* Monosynaptic restriction of transsynaptic tracing from single, genetically targeted neurons. *Neuron* **53,** 639–647 (2007).
10. Lafon, M. Rabies virus receptors. *J. Neurovirol.* **11,** 82–87 (2005).
11. Selemon, L. D. & Goldman-Rakic, P. S. The reduced neuropil hypothesis: a circuit based model of schizophrenia. *Biol. Psychiatry* **45,** 17–25 (1999).
12. Jaaro-Peled, H., Ayhan, Y., Pletnikov, M. V. & Sawa, A. Review of pathological hallmarks of schizophrenia: comparison of genetic models with patients and nongenetic models. *Schizophr. Bull.* **36,** 301–313 (2010).
13. Walsh, T. *et al.* Rare structural variants disrupt multiple genes in neurodevelopmental pathways in schizophrenia. *Science*320 539–543 (2008).
14. Higgs, B. W., Elashoff, M., Richman, S. & Barci, B. An online database for brain disease research. *BMC Genomics* **7,** 70 (2006).
15. Patil, S. T. *et al.* Activation of mGlu2/3 receptors as a new approach to treat schizophrenia: a randomized Phase 2 clinical trial. *Nature Med.* **13,** 1102–1107 (2007).
16. Patterson, S. L. *et al.* Some forms of cAMP-mediated long-lasting potentiation are associated with release of BDNF and nuclear translocation of phospho-MAP kinase. *Neuron* **32,** 123–140 (2001).
17. Freyberg, Z., Ferrando, S. J. & Javitch, J. A. Roles of the Akt/GSK-3 and Wnt signaling pathways in schizophrenia and antipsychotic drug action. *Am. J. Psychiatry* **167,** 388–396 (2010).
18. Stefansson, H. *et al.* Large recurrent microdeletions associated with schizophrenia. *Nature* **455,** 232–236 (2008).
19. The International Schizophrenia Consortium. Rare chromosomal deletions and duplications increase risk of schizophrenia. *Nature* **455,** 237–241 (2008).
20. Karayiorgou, M. & Gogos, J. A. The molecular genetics of the 22q11-associated schizophrenia. *Brain Res. Mol. Brain Res.* **132,** 95–104 (2004).
21. Wang, X. D., Su, Y. A., Guo, C. M., Yang, Y. & Si, T. M. Chronic antipsychotic drug administration alters the expression of neuregulin 1β, ErbB2, ErbB3, and ErbB4 in the rat prefrontal cortex and hippocampus. *Int. J. Neuropsychopharmacol.* **11,** 553–561 (2008).
22. Kapur, S. *et al.* PET evidence that loxapine is an equipotent blocker of 5-HT_2 and D_2 receptors: implications for the therapeutics of schizophrenia. *Am. J. Psychiatry* **154,** 1525–1529 (1997).
23. Cannon, T. D. & Keller, M. C. Endophenotypes in the genetic analyses of mental disorders. *Annu. Rev. Clin. Psychol.* **2,** 267–290 (2006).

Supplementary Information is linked to the online version of the paper at www.nature.com/nature.

Acknowledgements L. Moore, B. Miller, K. Stecker, J. Jepsen, D. Sepp, S. Larkin and L. Johnson provided technical assistance. T. Berggren directs, and M. Lutz manages, the Salk Stem Cell facility. D. Gibbs directs the Salk Viral Vector Core. J. Nguyen and L. Ouyang provided gene expression support. D. Chambers and J. Barrie provided FACS support. E. Callaway and I. Wickersham provided rabies trans-neuronal tracing viruses and invaluable advice and scientific feedback. M. Lawson provided assistance with statistical analysis. Thanks to G. Yeo, M. McConnell, S. Aigner, C. Marchetto and L. Boyer for advice and conversation. K.J.B. is supported by a training grant from the California Institute for Regenerative Medicine. The Gage Laboratory, and this project, is partially funded by CIRM Grant RL1-00649-1, The Lookout and Mathers Foundation, the Helmsley Foundation as well as Sanofi-Aventis.

Author Contributions K.J.B. designed the experiments with F.H.G. K.J.B. completed the experiments and wrote the manuscript. A.S. contributed to the microarray analysis and qPCR experiments. J.J. established the synaptic density assay and completed the calcium transient experiments. C.G.-B. and S.S. performed most of the synaptic protein experiments. N.T. analysed the rabies data. N.T. and S.S. together counted neurites. Y.L., Y.M. and G.C. performed electrophysiology. D.Y. established the calcium transient assay. S.M.C. and J.S. completed the CNV analysis.

Author Information The data discussed in this publication have been deposited in NCBI's Gene Expression Omnibus and are accessible through GEO Series accession number GSE25673. As per our agreement with Coriell Cell Repository, all hiPSC lines generated from control and schizophrenic fibroblasts will only be available from Coriell. Reprints and permissions information is available at www.nature.com/reprints. The authors declare no competing financial interests. Readers are welcome to comment on the online version of this article at www.nature.com/nature. Correspondence and requests for materials should be addressed to F.H.G. (gage@salk.edu).

METHODS

Description of SCZD patients. All patient samples were obtained from the Coriell collection. Patients were selected based on the high likelihood of a genetic component to disease. Patient 1 (GM02038, male, 22 years of age, Caucasian) was diagnosed with SCZD at 6 years of age and committed suicide at 22 years of age. Patient 2 (GM01792, male, 26 years of age, Jewish Caucasian) displayed episodes of agitation, delusions of persecution, and fear of assassination. His sister, patient 3 (GM01835, female, 27 years of age, Jewish Caucasian) had a history of schizoaffective disorder and drug abuse. Patient 4 (GM02497, male, 23 years of age, Jewish Caucasian) was diagnosed with SCZD at age 15 and showed symptoms including paralogical thinking, affective shielding, splitting of affect from content, and suspiciousness. His sister, patient 5 (GM02503, female, 27 years of age, Jewish Caucasian), was diagnosed with anorexia nervosa in adolescence and with schizoid personality disorder (SPD) as an adult. SPD has an increased prevalence in families with SCZD and is a milder diagnosis characterized not by psychosis, but rather by a lack of interest in social relationships and emotional coldness[24]. Although we show data from SPD patient 5 as an interesting point of comparison, we do not consider patient 5 to belong to either the 'control' or 'SCZD' groups.

Preliminary experiments were controlled using BJ fibroblasts from ATCC (CRL-2522). These fibroblasts were expanded from foreskin tissue of a newborn male. They are readily reprogrammed, low passage, karyotypically normal and extremely well-characterized primary fibroblast line cells. Age- and ancestry-matched controls were obtained from three Coriell collections: apparently healthy individuals with normal psychiatric evaluations, apparently healthy non-fetal tissue and gerontology research centre cell cultures. hiPSCs were generated from GM02937 (male, 22 years of age), GM03440 (male, 20 years of age), GM03651 (female, 25 years of age), GM04506 (female, 22 years of age), AG09319 (female, 24 years of age) and AG09429 (female, 25 years of age).

Generation of lentivirus. Lentivirus was packaged in 293T HEK cells grown in 293T medium (IMEM (Invitrogen), 10% FBS (Gemini), 1× GlutaMAX (Invitrogen)). 293T cells were transfected with polyethylenimine (PEI) (Polysciences). Per 15-cm plate, the following solution was prepared, incubated for 5 min at room temperature and added drop-wise to plates: 12.2 μg lentiviral DNA, 8.1 μg MDL-gagpol, 3.1 μg Rev-RSV, 4.1 μg CMV-VSVG, 500 μl of IMDM and 110 μl PEI (1 μg μl^{-1}) and vortexed lightly. Medium was changed after 3 h and the virus was harvested at 48 and 72 h post transfection.

hiPSC derivation. Human fibroblasts were cultured on plates treated with 0.1% gelatin (in milli-Q water) for a minimum of 30 min and grown in HF medium (DMEM (Invitrogen), 10% FBS (Gemini), 1× GlutaMAX (Invitrogen), 5 ng ml^{-1} FGF2 (Invitrogen)).

Human fibroblasts were infected daily for 5 days with tetracycline-inducible lentiviruses expressing *OCT4*, *SOX2*, *KLF4*, *cMYC* and *LIN28*, driven by a sixth lentivirus expressing the reverse tetracycline transactivator (rtTA)[7]. Cells from a single well of a 6-well dish were split onto a 10-cm plate containing 10^6 mouse embryonic fibroblasts (mEFs). Cells were switched to HUES medium (KO-DMEM (Invitrogen), 10% KO-Serum Replacement (Invitrogen), 10% Plasmanate (Talecris), 1× GlutaMAX (Invitrogen), 1× NEAA (Invitrogen), 1× 2-β-mercaptoethanol (Sigma) and 20 ng ml^{-1} FGF2 (Invitrogen)). Doxycycline (1 μg ml^{-1}; Sigma) was added to HUES medium for the first 21–28 days of reprogramming.

hiPSC colonies were picked manually and clonally plated onto 24-well mEF plates. hiPSC lines were either maintained on mEFs in HUES medium or on Matrigel (BD) in TeSR medium (StemCell Technologies). At early passages, hiPSCs were split through manual passaging. At higher passages, hiPSC could be enzymatically passaged with collagenase (1 mg ml^{-1} in DMEM; Sigma). Cells were frozen in freezing medium (DMEM, 10% FBS, 10% DMSO).

Karyotyping analysis was performed by Cell Line Genetics or by M. Dell'Aquila.

Teratoma analysis was performed by injecting hiPSCs into the kidney capsules of isoflurane-anesthetized NOD-SCID mice. Teratomas were harvested eight weeks post-injection, paraffin-embedded and stained with haematoxylin and eosin.

hiPSC differentiation to NPCs and neurons. hiPSCs grown in HUES medium on mEFs were incubated with collagenase (1 mg ml^{-1} in DMEM) at 37 °C for 1–2 h until colonies lifted from the plate and were transferred to a non-adherent plate (Corning). Embryoid bodies were grown in suspension in N2 medium (DMEM/F12-GlutaMAX (Invitrogen), 1× N2 (Invitrogen)). After 7 days, embryoid bodies were plated in N2 medium with 1 μg ml^{-1} laminin (Invitrogen) onto polyornithine (PORN)/laminin-coated plates. Visible rosettes formed within one week and were manually dissected onto PORN/laminin-coated plates. Rosettes were cultured in NPC medium (DMEM/F12, 1x N2, 1x B27-RA (Invitrogen), 1 μg ml^{-1} Laminin and 20 ng ml^{-1} FGF2) and dissociated in TrypLE (Invitrogen) for 3 min at 37 °C. NPCs are maintained at high density, grown on PORN/laminin-coated plates in NPC medium and split approximately 1:4 every week with Accutase (Millipore).

For neural differentiations, NPCs were dissociated with Accutase and plated in neural differentiation medium (DMEM/F12, 1× N2, 1× B27-RA, 20 ng ml^{-1} BDNF (Peprotech), 20 ng ml^{-1} GDNF (Peprotech), 1 mM dibutyryl-cyclic AMP (Sigma), 200 nM ascorbic acid (Sigma) onto PORN/laminin-coated plates. Density is critical and the following guidelines were used: 2-well Permanox slide, 80,000–100,000 cells per well; 24-well, 40,000–60,000 cells per well; 6-well, 200,000 cells per well. hiPSC-derived neurons were differentiated for 1–3 months. Notably, synapse maturation occurs most robustly *in vitro* when hiPSC neurons are cultured together with wild-type human cerebellar astrocytes (ScienCell). FBS (0.5%) was supplemented into neural differentiation media for all astrocyte coculture experiments.

It is difficult to maintain healthy neurons for 3 months of differentiation and some cultures invariably fail or become contaminated. When even one SCZD patient neural culture failed, the experiments were abandoned as all assays were conducted on neurons cultured in parallel. If, however, only a control neural culture failed, and at least three control samples remained, analysis was completed. For this reason, although patients are consistently numbered throughout the manuscript, controls are not, and are instead listed in numerical order (BJ, GM02937, GM03651, GM04506, AG09319, AG09429).

Antipsychotic drugs were added for the final 3 weeks of a 3-month differentiation on astrocytes and for the final two weeks of a 6-week differentiation on PORN/laminin alone. Drugs were resuspended in DMSO at the following concentrations: clozapine (5 μM), loxapine (10 μM), olanzapine (1 μM), risperidone (10 μM) and thioridazine (5 μM).

Immunohistochemistry. Cells were fixed in 4% paraformaldehyde in PBS at 4 °C for 10 min. hiPSCs and NPCs were permeabilized at room temperature for 15 min in 1.0% Triton in PBS. All cells were blocked in 5% donkey serum with 0.1% Triton at room temperature for 30 min. The following primary antibodies and dilutions were used: mouse anti-Oct4 (Santa Cruz), 1:200; goat anti-Sox2 (Santa Cruz), 1:200;goat anti-Nanog (R&D), 1:200; mouse anti-Tra1-60 (Chemicon), 1:100; mouse anti-human Nestin (Chemicon), 1:200; rabbit anti-βIII-tubulin (Covance), 1:200; mouse anti-βIII-tubulin (Covance), 1:200; rabbit anti-cow-GFAP (Dako) 1:200; mouse anti-MAP2AB (Sigma), 1:200; rabbit anti-synapsin (Synaptic Systems), 1:500; mouse anti-PSD95 (UCDavis/NIH Neuromab), 1:500; rabbit anti-PSD95 (Invitrogen), 1:200 rabbit-anti-VGLUT1 (Synaptic; Systems), 1:500; rabbit anti-gephyrin, (Synaptic Systems), 1:500; mouse anti-vGAT (Synaptic Systems), 1:500; rabbit anti-vGat (Synaptic Systems), 1:500; rabbit anti-GLUR1 (Oncogene), 1:100; rabbit anti-GABA (Sigma), 1:200; rabbit anti-GAD65/67 (Sigma), 1:200.

Secondary antibodies were Alexa donkey 488, 555 and 647 anti-rabbit (Invitrogen), Alexa donkey 488 and 555 anti-mouse (Invitrogen), and Alexa donkey 488, 555, 568 and 594 anti-goat (Invitrogen); all were used at 1:300. To visualize nuclei, slides were stained with 0.5 μg ml^{-1} DAPI (4′,6-diamidino-2-phenylindole) and then mounted with Vectashield. Images were acquired using a Bio-Rad confocal microscope.

FACS. For sorting of dissociated two-month-old hiPSC neurons, cultures were dissociated with Accutase for 5 min, washed in DMEM, centrifuged at 500*g* and resuspended in PBS. Cells were fixed in 4% paraformaldehyde in PBS at 4 °C for 10 min. Cells were washed in PBS and aliquoted into 96-well conical plates. Cells were blocked in 5% donkey serum with 0.1% saponin at room temperature for 30 min. The following primary antibodies and dilutions were used for one hour at room temperature: rabbit anti-βIII-tubulin (Sigma), 1:200; mouse anti-βIII-tubulin (Covance), 1:200; rabbit anti-GAD56/67 (Sigma), 1:200. Cells were washed and then incubated with secondary antibodies at 1:200 for 30 min at room temperature: Alexa donkey 647 anti-rabbit (Invitrogen), and Alexa donkey 488 anti-mouse (Invitrogen). Cells were washed three times in PBS and stained with 0.5 μg ml^{-1} DAPI. Cells were resuspended in PBS with 5% donkey serum and 0.1% detergent saponin. The homogeneous solution was filtered through a 250-μm nylon sieve and run in a BD FACSCalibur. Data were analysed using FloJo.

Rabies virus trans-neuronal tracing. Rabies virus trans-neuronal tracing was performed on 3-month-old hiPSC neurons grown together with wild-type human astrocytes (ScienCell) on acid-etched glass coverslips and then transduced with LV-SYNP-HTG or LV-SYNP-HT. Cultures were transduced with Rabies-ENVAΔG-RFP after at least a week to allow expression of ENVA and rabies G. Either 5, 7 or 10 days later, hiPSC neurons were fixed with 4% paraformaldehyde in PBS for fluorescent microscopy or FACS analysis; cells for FACS analysis were first dissociated with Accutase before fixation.

Neurite analysis. Neurite analysis was performed on 3-month-old hiPSC neurons grown together with wild-type human astrocytes (ScienCell) on acid-etched glass coverslips. Low titre transduction of a lentivirus driving expression of GFP from the SYN promoter (LV-SYNP-GFP) occurred at least 7 days before assay. LV-SYNP-GFP was used to image and count branching neurites from single neurons

(Fig. 3a). The number of neurites extending from the soma of 691 single LV-SYNP-GFP-labelled neurons was determined by a blinded count.

Synaptic protein staining analysis. Synaptic protein staining was performed on 3-month-old hiPSC neurons grown together with wild-type human astrocytes (ScienCell) on acid-etched glass coverslips. To calculate ratios of MAP2AB-positive dendrites and synaptic proteins, confocal images were taken at ×630 magnification and ×4 zoom. Using NIH ImageJ, images were thresholded and the integrated pixel density was determined for each image. Integrated pixel density measurement is the product of area (measured in square pixels) and mean grey value (the sum of the grey values of all the pixels in the selection divided by the number of pixels).

Synapse density. Synapse density analysis was performed on 3-month-old hiPSC neurons grown together with wild-type human astrocytes (ScienCell) on acid-etched glass coverslips. Manual counts of synaptic density were done in three steps using NIH ImageJ. First, the colocalization plugin was used to identify colocalization of VGLUT1 and PSD95. Second, the particle analysis function was used to restrict size 50-infinity. Third, dendrites were traced using the NeuronJ plugin. The mask generated by particle analysis was overlaid on the trace generated by NeuronJ and synapses were manually counted.

Electrophysiology. Whole-cell perforated patch recordings were performed on SCZD ($n = 30$) and control ($n = 20$) 3-month-old hiPSC neurons grown together with wild-type human astrocytes (ScienCell) on acid-etched coverslips and typically transduced with LV-SYNP-GFP. The recording micropipettes (tip resistance 3–6 MΩ) were tip-filled with internal solution composed of 115 mM K-gluconate, 4 mM NaCl, 1.5 mM $MgCl_2$, 20 mM HEPES, and 0.5 mM EGTA (pH 7.4) and then back-filled with the same internal solution containing 200 μg ml^{-1} amphotericin B (Calbiochem). Recordings were made using an Axopatch 200B amplifier (Axon Instruments). Signals were sampled and filtered at 10 kHz and 2 kHz, respectively. The whole-cell capacitance was fully compensated, whereas the series resistance was uncompensated but monitored during the experiment by the amplitude of the capacitive current in response to a 5-mV pulse. The bath was constantly perfused with fresh HEPES-buffered saline composed of 115 mM NaCl, 2 mM KCl, 10 mM HEPES, 3 mM $CaCl_2$, 10 mM glucose and 1.5 mM $MgCl_2$ (pH 7.4). For voltage-clamp recordings, cells were clamped at −60 to −80 mV; Na^+ currents and K^+ currents were stimulated by voltage step depolarizations. Command voltage varied from −50 to +20 mV in 10 mV increments. For current-clamp recordings, induced action potentials were stimulated with current steps from −0.2 to +0.5 nA. All recordings were performed at room temperature.

Spontaneous calcium transients. Calcium imaging analysis was performed on 2.5- to 3-month-old hiPSC neurons grown together with wild-type human astrocytes (ScienCell) on acid-etched glass coverslips. Culture medium was removed and hiPSC cultures were incubated with 0.4 μM Fluo-4AM (Molecular Probes) and 0.02% Pluronic F 127 detergent in Krebs HEPES buffer (KHB) (10 mM HEPES, 4.2 mM $NaHCO_3$, 10 mM dextrose, 1.18 mM $MgSO_4 \cdot 2H_2O$, 1.18 mM KH_2PO_4, 4.69 mM KCl, 118 mM NaCl, 1.29 mM $CaCl_2$; pH 7.3) for 1 h at room temperature. Cells were washed with KHB buffer, incubated for 2 min with Hoechst dye diluted 1:1,000 in KHB, and allowed to incubate for an additional 15 min in KHB to equilibrate intracellular dye concentration. Time-lapse image sequences (×100 magnification) were acquired at 28 Hz using a Hamamatsu ORCA-ER digital camera with a 488-nm (FITC) filter on an Olympus IZ81 inverted fluorescence confocal microscope. Images were acquired with MetaMorph.

In total, eight independent neural differentiations were tested per patient, 210 movies of spontaneous calcium transients (110 control and 100 SCZD) were generated and 2,676 regions of interest (1,158 control and 1,518 SCZD) were analysed. Up to four 90-s videos of Fluo-4AM fluorescence were recorded per neural differentiation per patient with a spinning disc confocal microscope at 28 frames per second (Supplementary Fig. 5A). Using ImageJ software, regions of interest can be manually selected and the mean pixel intensity of each regions of interest can be followed over time, generating time trace data for each regions of interest. The data were analysed in Matlab where background subtraction was performed by normalizing traces among traces of the sample, and spike events were identified based on the slope and amplitude of the time trace.

The amplitude of spontaneous calcium transients was calculated by measuring the change in total pixel intensity for each normalized calcium transient trace. The rate was determined by dividing the total number of spontaneous calcium transients for any regions of interest by the total length of the movie (90 s). The synchronicity of spontaneous calcium transients was determined by two independent calculations. First, to determine the percentage synchronicity per calcium transient, the total number of synchronized calcium transients, defined as three or more simultaneous peaks, was divided by the total number of spontaneous calcium transients identified. Second, to calculate the maximum percentage synchronicity, the maximum number of regions of interest involved in a single synchronized event was divided by the total number of regions of interest identified.

CNV analysis. Cells were lysed in DNA lysis solution (100 mM Tris, pH 8.5, 5 mM EDTA, 200 mM NaCl, 0.2% (w/v) sarcosyl and 100 μg ml^{-1} fresh proteinase K) overnight at 50 °C. DNA was precipitated by the addition of an equal volume of NaCl-ethanol mixture (150 μl of 5 M NaCl in 10 ml cold 95% ethanol) and then washed three times in 70% ethanol before resuspension in water with RNase A overnight at 4 °C.

Genome scans were performed using NimbleGen HD2 arrays (NimbleGen Systems) according the to the manufacturer's instructions using a standard reference genome SKN1. NimbleGen HD2 dual-colour intensity data were normalized in a two-step process: first, a 'spatial' normalization of probes was performed to adjust for regional differences in intensities across the surface of the array; second, the Cy5 and Cy3 intensities were adjusted to a fitting curve by invariant set normalization, preserving the variability in the data. The $\log_2$ ratio for each probe was then estimated using the geometric mean of normalized and raw intensity data[25].

CNV analysis was completed to identify deletions and duplications present within our patients. By using a virtual 'genotyping' step whereby individual CNV segment probe ratios were converted into *z*-scores, a distribution of median *z*-scores was generated, outliers of which were considered to be true CNVs. In doing so, we better filtered out common artefacts and false-positive CNVs and generated a list of CNVs unbiased by previous genetic studies of SCZD.

Patient fibroblasts were used for CNV analysis. Lymphocytes were available for patients 4 and 5 and their parents, allowing us to validate the CNVs identified for patient 4 and also to determine the parent of origin for each mutation; many were inherited from the unaffected mother (Supplementary Table 7).

Gene expression analysis. Unless otherwise specified, gene expression analysis was performed on 6-week-old hiPSC neurons without astrocyte coculture. Cells were lysed in RNA BEE (Tel-test). RNA was chloroform-extracted, pelleted with isopropanol, washed with 70% ethanol and resuspended in water. RNA was treated with RQ1 RNase-free DNase (Promega) for 30 min at 37 °C and then the reaction was inactivated by incubation with EGTA stop buffer at 65 °C for 10 min.

For gene expression microarrays, three independent neural differentiations for each of the four SCZD patients as well as four control subjects were compared using Affymetrix Human 1.0ST arrays as specified by the manufacturer.

Gene expression microarray analysis was completed using Partek Genomics Suite software. Intensity values were generated as follows: RMA background correction, quantile normalization, $\log_2$ transformation and mean polished probeset summarization. Pathway analysis was performed using Metacore GeneGo.

For qPCR, cDNA was synthesized using Superscript III at 50 °C for 1–2 h, inactivated for 15 min at 70 °C and then treated with RNase H for 15 min at 37 °C, inactivated with EDTA and heated to 70 °C for 15 min. qPCR was performed using SYBR Green. Primers used are listed in Supplementary Table 8.

Statistical analysis. Statistical analysis was performed using JMP. Box-Cox transformation of raw data was performed to correct non-normal distribution of the data and residuals. Improvements were assessed by Shapiro–Wilk *W* test of the transformed data and residuals. Means were compared within diagnosis by one-way analysis using both Student's *t*-test and Tukey–Kramer HSD. Finally, a nested analysis of values for individual patients was performed using standard least squares analysis comparing means for all pairs using Student's *t*-test for specific pairs and Tukey–Kramer HSD for multiple comparisons.

24. American Psychiatric Association. *Diagnostic and statistical manual of mental disorders, fourth edition (DSM-IV).* (American Psychiatric Press, 1994).
25. McCarthy, S. E. *et al.* Microduplications of 16p11.2 are associated with schizophrenia. *Nature Genet.* **41,** 1223–1227 (2009).

CORRIGENDUM

doi:10.1038/nature10603

Modelling schizophrenia using human induced pluripotent stem cells

Kristen J. Brennand, Anthony Simone, Jessica Jou, Chelsea Gelboin-Burkhart, Ngoc Tran, Sarah Sangar, Yan Li, Yangling Mu, Gong Chen, Diana Yu, Shane McCarthy, Jonathan Sebat & Fred H. Gage

Nature **473,** 221–225 (2011)

In this Letter, the scale bars were calculated incorrectly for each image throughout the manuscript and 60× objectives were reported as 63×. Although all the images are correct as published, the length represented by every scale bar was wrong. The figure legends for Fig. 1 (the three scale bars are now all 100 μm and '×630' should be '×600') and Fig. 2 (the scale bar is now 80 μm) have been amended in the PDF and HTML versions online. Similar errors in Supplementary Figs 2–5 and 7–10 have also been corrected online. We very much regret these errors. These changes do not alter any of the conclusions of this Letter.